A Simulation Framework for Humeral Head Translations

Ehsan Sarshari[a,b], Alain Farron[c], Alexandre Terrier[b], Dominique Pioletti[b], Philippe Mullhaupt[a,*]

[a] *Automatic Control Laboratory, Ecole Polytechnique Fédérale de Lausanne (EPFL), Switzerland*
[b] *Laboratory of Biomechanical Orthopedics, Ecole Polytechnique Fédérale de Lausanne (EPFL), Switzerland*
[c] *Department of Orthopedics and Traumatology, University Hospital Centre and University of Lausanne (CHUV), Switzerland*

Abstract

Humeral head translations (HHT) play a crucial role in the glenohumeral (GH) joint function. The available shoulder musculoskeletal models developed based on inverse dynamics however fall short of predicting the HHT. This study aims at developing a simulation framework that allows forward-dynamics simulation of a shoulder musculoskeletal model with a 6 degrees of freedom (DOF) GH joint. It provides a straightforward solution to the HHT prediction problem. We show that even within a forward-dynamics simulation addressing the HHT requires further information about the contact. To that end, a deformable articular contact is included in the framework defining the GH joint contact force in terms of the joint kinematics. An abduction motion in the scapula plane is simulated. The results are given in terms of HHT, GH joint contact force, contact areas, contact pressure, and cartilage strain. It predicts a superior-posterior translation of the humeral head followed by an inferior migration.

Keywords: Shoulder musculoskeletal model, Humeral head translations, Glenohumeral joint, Forward-dynamics simulation, Deformable articular contact

1. Introduction

Several musculoskeletal models are available for the human shoulder that provide reliable predictions of both the muscle and joint reaction forces e.g. [1, 2]. A vast majority of these models have been developed based on inverse dynamics, e.g. [2–7]. In inverse dynamics, measured joints kinematics (rotations and translations) are required as inputs to calculate muscle and joint reaction

*Corresponding author at: Automatic Control Laboratory, Ecole Polytechnique Fédérale de Lausanne, Station 9, 1015 Lausanne, Switzerland. Tel.: +41 21 69 33838 ; fax: +41 21 69 32574.

Email address: `philippe.muellhaupt@epfl.ch` (Philippe Mullhaupt)

forces. However, with the available measurement techniques, it is not straightforward to measure the translational DOF of the GH joint [8]. Therefore, it is often approximated as an ideal ball-and-socket joint in the musculoskeletal models, neglecting its translation [9]. A so-called stability constraint is also often considered in the load-sharing scheme of the models to restrict the GH joint reaction force to point into the glenoid fossa, avoiding subluxations by enforcing more physiological contributions from the rotator cuff muscles [1]. Nonetheless, the GH joint translations have a role to play in the GH joint stability mechanism [1, 10]. Furthermore, predictions of the GH joint translations, the contact pressure, and the contact areas are required in designing shoulder prostheses [11, 12].

Indeed, few studies have investigated the HHT using biomechanical models. To this end, they tailored either available musculoskeletal models [12, 13] or developed finite element models [9, 11, 14, 15]. Other studies mainly used cadaveric [16, 17] or clinical [8, 18–23] approaches to address the GH joint translations. However, there are limitations associated to each of these studies. The Anybody shoulder model [6] was tailored using the force dependent kinematic method, introduced in [24], to address the HHT after total shoulder arthroplasty (TSA) [12]. The dynamic effects of motion were neglected although their influence on the HHT has been already highlighted [18]. A shoulder model, developed in [25], was adapted in [13] to address the HHT using a novel inverse-dynamics framework. The HHT was considered as an extra design variable in an optimization scheme within this framework. Despite [12], the dynamic effects of motion were partially considered. However, the articular contact was approximated by an elastic potential function. This deviates from the nonlinear and viscoelastic behavior of the cartilage [26] and does not account for the moment applied on the humerus due to the articular contact. The different 3D finite element models developed in [9, 11, 14, 15] share the same attributes. They include more realistic estimation for the articular contact although they were simulated under a sequence of static conditions, neglecting the dynamics of motion. Furthermore, they all lack a physiological muscle force load-sharing. The 3D finite element model developed in [9] was used in[10, 27, 28] to further study the HHT after the TSA.

The *in vivo* or *in vitro* measurement of the HHT remains a challenging task [8]. Specifically, *in vitro* studies cannot accurately simulate the *in vivo* conditions in terms of the muscle and joint contact forces. The *in vivo* studies are also either limited to 2 dimensional analysis [18, 19] or otherwise their accuracy is limited by the 3D reconstruction of the bones [8, 22, 23]. Furthermore, they are not developed to assess the GH joint translations during dynamic activities [20, 21].

The aim of this study is to develop a simulation framework for a shoulder musculoskeletal model that allows simultaneous predictions of HHT, joint reaction forces, and contact pressure. To that end, a forward-dynamics simulation coupled with a nonlinear viscoelastic approximation of the articular contact is used. The dynamic equations of motion are therefore solved forward in time, allowing a straightforward consideration of the dynamic effects of the motion. To the best of our knowledge this has not been addressed elsewhere. This simulation

framework provides addressing the GH joint kinematics (HHT) and mechanics (reaction forces and contact pressure) either in its physiological form or after the TSA. The outcome of this simulation framework will be translated for future patient-specific clinical applications related to the treatment of osteoarthritis by TSA.

2. Methods

A musculoskeletal model of the GH joint with 6 DOF is developed. The 6 DOF correspond to 3 rotational and 3 translational (HHT) generalized coordinates. We show that the equations of motion of the GH joint with 6 DOF is indeterminate, i.e. there are fewer equations than the number of unknown forces and unknown generalized coordinates (subsection 2.1). Therefore, defining the HHT requires solving the indeterminate equations of motion of the GH joint. In order to resolve the indeterminacy, we develop a framework that maps the unknown forces to the unknown generalized coordinates and velocities (subsections 2.3 and 2.3). This leads to a set of transformed equations of motion that no longer is indeterminate. We then simulate an arm motion in the scapula plane. The resulted HHT, GH joint contact force, contact areas, contact pressure, and cartilage strain are compared to those from the *in vitro*, *in vivo*, and numerical studies.

2.1. Indeterminacy in HHT

The surfaces of humeral head and glenoid fossa are both approximated as spheres with radii r_h and r_g equal to 30 [mm] and 32 [mm], respectively [29] (Fig. 1). The arm weight is 35.7 [N] that corresponds to 5% of the bodyweight. All the 11 major muscles spanning the GH joint are included, and their forces applied on the humerus are replicated by a resultant force $\boldsymbol{F}_m$ and a resultant moment $\boldsymbol{M}_m$ acting on the humeral head center. Muscle paths are defined using the algorithm introduced in [4]. $\boldsymbol{F}_c$ represents the GH joint contact force applied on the humerus. The contact point on the humeral head and its associate point on the glenoid fossa are denoted by $\boldsymbol{C}_h$ and $\boldsymbol{C}_g$, with velocities of $\boldsymbol{V}_{C_h}$ and $\boldsymbol{V}_{C_g}$, respectively. x_h, y_h, and z_h are the humerus body-fixed coordinates at the humeral head center ($\boldsymbol{HH}$). The scapula motion is included by the scapulohumeral rhythm [30].

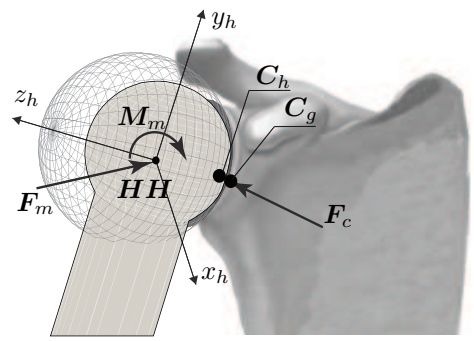

Figure 1: A schematic view of the GH joint. The surfaces of humeral head and the glenoid fossa are both approximated as spheres. x_h, y_h, and z_h are the humerus body-fixed coordinates attached to the humeral head center $\boldsymbol{HH}$. $\boldsymbol{F}_m$ and $\boldsymbol{M}_m$ are resultant force and moment due to the muscles, and $\boldsymbol{F}_c$ is the contact force. The contact points on the humeral head and the glenoid fossa are denoted by $\boldsymbol{C}_h$ and $\boldsymbol{C}_g$, respectively.

The GH joint equations of motion are derived using the Lagrange's equations. A compact form of these equations is

$$\frac{d}{dt}\left(\frac{\partial L}{\partial \dot{\boldsymbol{q}}}\right) - \frac{\partial L}{\partial \boldsymbol{q}} = \boldsymbol{\tau}(\boldsymbol{F}_m, \boldsymbol{F}_c) \tag{1}$$

The generalized coordinate vector $\boldsymbol{q}$ consists of three rotational DOF (ψ, θ, and ϕ) and three translational DOF (x, y, and z). The generalized force vector $\boldsymbol{\tau}$ is a function of applied external forces ($\boldsymbol{F}_m$ and $\boldsymbol{F}_c$) [31]. A holonomic constraint is also considered to account for the contact between the surfaces of humeral head and glenoid fossa

$$(\boldsymbol{V}_{C_h} - \boldsymbol{V}_{C_g}) \,.\, \hat{\boldsymbol{n}} = 0 \tag{2}$$

The unit vector $\hat{\boldsymbol{n}}$ is perpendicular to the plane of contact that is tangential to the contact point. The constraint equation assures no relative velocity between $\boldsymbol{C}_h$ and $\boldsymbol{C}_g$ in the direction of $\hat{\boldsymbol{n}}$ [32].

There are 12 unknowns in equations (1) and (2), including the 6 generalized coordinates (ψ, θ, ϕ, x, y, and z), the 3 components of the contact force ($\boldsymbol{F}_c$), and the 3 components of the resultant muscle force ($\boldsymbol{F}_m$). However, equations (1) and (2) respectively provide 6 and 1 equations (7 in total) that are not sufficient to uniquely determine the 12 unknowns. Therefore, the equations of motion of the GH joint with 6 DOF is indeterminate.

2.2. Resolving the indeterminacy: deformable articular contact

Our approach to resolve the indeterminacy is to define the unknown muscle and contact forces and their associated moments as smooth function mappings of the generalized coordinate and velocity vectors. This leads to a set of transformed equations of motion that is no longer indeterminate.

Using the definition of virtual work [31], the generalized force vector ($\boldsymbol{\tau}$) on the right-hand side of (1) can be expressed as

$$\boldsymbol{\tau} = (\boldsymbol{F}_m + \boldsymbol{F}_c)\frac{\partial \boldsymbol{V}_{HH}}{\partial \dot{\boldsymbol{q}}} + (\boldsymbol{M}_{HH_m} + \boldsymbol{M}_{HH_c})\frac{\partial \boldsymbol{\omega}}{\partial \dot{\boldsymbol{q}}} \tag{3}$$

where $\boldsymbol{V}_{HH}$ is the velocity of the humeral head center, and $\boldsymbol{\omega}$ is the angular velocity of the humerus. $\boldsymbol{M}_{HH_m}$ and $\boldsymbol{M}_{HH_c}$ denote the resultant moments about the humeral head center due to the muscle and the contact forces, respectively.

Substituting $\boldsymbol{F}_c$, $\boldsymbol{F}_m$, $\boldsymbol{M}_{HH_c}$, and $\boldsymbol{M}_{HH_m}$ in (3) with smooth function mappings (to be defined) of $\boldsymbol{q}$ and $\dot{\boldsymbol{q}}$ and introducing the resulting generalized force vector into (1), we obtain

$$\begin{aligned} \frac{d}{dt}\left(\frac{\partial L}{\partial \dot{\boldsymbol{q}}}\right) - \frac{\partial L}{\partial \boldsymbol{q}} = \mathscr{F}_c(\boldsymbol{q}, \dot{\boldsymbol{q}})\frac{\partial \boldsymbol{V}_{HH}}{\partial \dot{\boldsymbol{q}}} + \mathscr{M}_{HH_c}(\boldsymbol{q}, \dot{\boldsymbol{q}})\frac{\partial \boldsymbol{\omega}}{\partial \dot{\boldsymbol{q}}} \\ + \mathscr{F}_m(\boldsymbol{q}, \dot{\boldsymbol{q}})\frac{\partial \boldsymbol{V}_{HH}}{\partial \dot{\boldsymbol{q}}} + \mathscr{M}_{HH_m}(\boldsymbol{q}, \dot{\boldsymbol{q}})\frac{\partial \boldsymbol{\omega}}{\partial \dot{\boldsymbol{q}}} \end{aligned} \tag{4}$$

where $\mathscr{F}_c$, $\mathscr{F}_m$, $\mathscr{M}_{HH_c}$, and $\mathscr{M}_{HH_m}$ are the smooth function mappings from $\boldsymbol{q}$ and $\dot{\boldsymbol{q}}$ to $\boldsymbol{F}_c$, $\boldsymbol{F}_m$, and their associated moments. Once these function mappings are defined, solving the transformed equations of motion (4) is trivial.

To define $\mathscr{F}_c$, a deformable articular contact between the humeral head and the glenoid fossa is assumed. This contradicts our previous contact constraint in (2) where a rigid contact was assumed. However, the assumption of a deformable articular contact is more physiologically consistent [1, 33] and allows us to define $\mathscr{F}_c$. The deformable contact model used here is adapted from [34] approximating the cartilage as a nonlinear elastic material. A viscous damping term is also incorporated to this contact model according to [33]. The humeral head is considered to be rigid while a deformable layer covers the glenoid fossa (Fig. 2). The thickness of this deformable layer accounts for the cartilage of both humeral head and glenoid fossa. The vector $\boldsymbol{r}_{HH}$ defines the position of the humeral head center in the scapula coordinates (x_s, y_s, and z_s). We denote respectively by ${}^s\boldsymbol{h}_i$ and $\boldsymbol{h}_i$ the center point of an infinitesimal surface on the humeral head in the scapula and humerus frames and by $\boldsymbol{f}_{c_i}$ its associated contact force. According to [34] and [33], the contact force applied on $\boldsymbol{h}_i$ can be express as

$$\boldsymbol{f}_{c_i} = \begin{cases} (a_i\, s\, \mathrm{Ln}\left(1 - \frac{u_i}{b}\right) + c\,\dot{u}_i)\frac{{}^s\boldsymbol{h}_i}{|{}^s\boldsymbol{h}_i|} & , \quad u_i > 0 \\ \boldsymbol{0} & , \quad u_i \leq 0 \end{cases} \tag{5}$$

where a_i, s, b, and c are the infinitesimal surface area, the aggregate module, the cartilage thickness, and the damping coefficient, respectively. We denote by u_i the amount that $\boldsymbol{h}_i$ penetrates the sphere approximating the glenoid fossa. Therefore, u_i is defined as $(|{}^s\boldsymbol{h}_i| - r_g)$ where ${}^s\boldsymbol{h}_i$ is $(\boldsymbol{r}_{HH} + R_{H,S}\boldsymbol{h}_i)$ with $R_{H,S}$ being the rotation matrix from the humerus coordinate to the scapula coordinate. The numerical values for the constants are adapted from the literature [9, 26, 35].

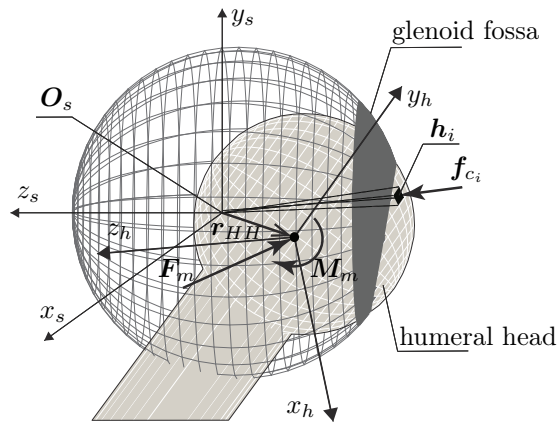

Figure 2: The GH joint with deformable articular contact (the dimensions are exaggerated for illustrations purposes). $\boldsymbol{r}_{HH}$ defines the spatial position of the humeral head in the scapula coordinates (x_s, y_s, and z_s). The center point of an infinitesimal surface on the humeral head in the humerus frames is denoted by $\boldsymbol{h}_i$, and $\boldsymbol{f}_{c_i}$ denotes its associated contact force.

2.3. Resolving the indeterminacy: forward-dynamics simulation

Having defined the function mapping $\mathscr{F}_c$, we here develop a forward-dynamics framework to define $\mathscr{M}_{HH_m}$. The forward-dynamics framework is a continuation of our previous work [36]. We define $\mathscr{M}_{HH_m}$ and accordingly $\boldsymbol{M}_{HH_m}$ such that the rotational generalized coordinates and velocities ($\boldsymbol{q}_r$ and $\dot{\boldsymbol{q}}_r$) follow their associated desired trajectory ($\boldsymbol{q}_{r_d}$ and $\dot{\boldsymbol{q}}_{r_d}$). To that end, we expand the transformed equations of motion (4) and split it into rotational and translational subspaces ($\boldsymbol{q}_r$ and $\boldsymbol{q}_t$):

$$\begin{aligned}\begin{bmatrix} M_{11} & M_{12} \\ M_{12} & M_{22} \end{bmatrix} \begin{bmatrix} \ddot{\boldsymbol{q}}_r \\ \ddot{\boldsymbol{q}}_t \end{bmatrix} + \boldsymbol{c}(\boldsymbol{q}, \dot{\boldsymbol{q}}) + \boldsymbol{g}(\boldsymbol{q}) - \mathscr{F}_c \frac{\partial \boldsymbol{V}_{HH}}{\partial \dot{\boldsymbol{q}}} - \mathscr{M}_{HH_c} \frac{\partial \boldsymbol{\omega}}{\partial \dot{\boldsymbol{q}}} \\ = \mathscr{F}_m \frac{\partial \boldsymbol{V}_{HH}}{\partial \dot{\boldsymbol{q}}} + \mathscr{M}_{HH_m} \frac{\partial \boldsymbol{\omega}}{\partial \dot{\boldsymbol{q}}}\end{aligned} \tag{6}$$

where $[M]$, $\boldsymbol{c}$, and $\boldsymbol{g}$ are the inertia matrix, centrifugal and Coriolis torques vector, and gravitational torques vector, respectively. $\mathscr{F}_c$ and consequently $\mathscr{M}_{HH_c}$ are already defined in subsection 2.2.

A change of coordinates is performed according to [37] to decouple (6). We denote by $\boldsymbol{f}_m$ a vector that consists of the magnitudes of the forces applied by different muscles. Two matrices B and W are also defined that map $\boldsymbol{f}_m$ to $\boldsymbol{F}_m$ and $\boldsymbol{M}_{HH_m}$, respectively. B is the matrix composed of the muscle force directions, and W is the moment arm matrix. Making these substitutions and denoting by $\boldsymbol{L}$ the four last terms on the left-hand side of (6), we obtain

$$\begin{bmatrix} M_{11} & 0 \\ 0 & M_{22} \end{bmatrix} \begin{bmatrix} \ddot{\boldsymbol{q}}_r \\ \ddot{\boldsymbol{q}}_t \end{bmatrix} + \begin{bmatrix} \boldsymbol{L}_r(\boldsymbol{q}, \dot{\boldsymbol{q}}) \\ \boldsymbol{L}_t(\boldsymbol{q}, \dot{\boldsymbol{q}}) \end{bmatrix} = B\boldsymbol{f}_m \frac{\partial \boldsymbol{V}_{HH}}{\partial \dot{\boldsymbol{q}}} + W\boldsymbol{f}_m \frac{\partial \boldsymbol{\omega}}{\partial \dot{\boldsymbol{q}}} \tag{7}$$

Defining B_g as $B\frac{\partial \boldsymbol{V}_{HH}}{\partial \dot{\boldsymbol{q}}}$ and W_g as $W\frac{\partial \boldsymbol{\omega}}{\partial \dot{\boldsymbol{q}}}$, and eliminating their zero raws accordingly, yields

$$\begin{bmatrix} M_{11} & 0 \\ 0 & M_{22} \end{bmatrix} \begin{bmatrix} \ddot{\boldsymbol{q}}_r \\ \ddot{\boldsymbol{q}}_t \end{bmatrix} + \begin{bmatrix} \boldsymbol{L}_r(\boldsymbol{q}, \dot{\boldsymbol{q}}) \\ \boldsymbol{L}_t(\boldsymbol{q}, \dot{\boldsymbol{q}}) \end{bmatrix} = \begin{bmatrix} W_g \boldsymbol{f}_m \\ B_g \boldsymbol{f}_m \end{bmatrix} \tag{8}$$

Equation (8) allows us to define the magnitudes of the muscle forces such that the humerus follows a desired rotational trajectory. The rotational subspace of the transformed equations of motion (8) is

$$M_{11}\ddot{\boldsymbol{q}}_r + \boldsymbol{L}_r(\boldsymbol{q}, \dot{\boldsymbol{q}}) = W_g \boldsymbol{f}_m \tag{9}$$

where it can be solved for $\ddot{\boldsymbol{q}}_r$

$$\ddot{\boldsymbol{q}}_r = {M_{11}}^{-1}(W_g \boldsymbol{f}_m - \boldsymbol{L}_r(\boldsymbol{q}, \dot{\boldsymbol{q}})) \tag{10}$$

The right-hand side of (10) is considered as a new intermediate control input $\boldsymbol{v}$ [38]. This results in an equivalent linear system

$$\ddot{\boldsymbol{q}}_r = \boldsymbol{v} \tag{11}$$

We define the tracking error as $\widetilde{\boldsymbol{q}}_r = \boldsymbol{q}_r - \boldsymbol{q}_{r_d}$. Letting

$$\boldsymbol{v} = \ddot{\boldsymbol{q}}_{r_d} - 2\lambda\dot{\widetilde{\boldsymbol{q}}}_r - \lambda^2\widetilde{\boldsymbol{q}}_r \quad , \quad \lambda > 0 \tag{12}$$

results in an exponentially stable closed-loop dynamics for (11). Having defined $\boldsymbol{v}$, the function mapping $\mathscr{M}_{HH_m}$ and accordingly $W_g \boldsymbol{f}_m$ can be achieved by substituting $\ddot{\boldsymbol{q}}_r$ from (11) into (9). Given that the raw size of $\boldsymbol{f}_m$ is larger than the rank of W_g, a static optimization is used to arrive at a set of nontrivial muscle force magnitudes ($\boldsymbol{f}_m$):

$$\begin{array}{ll} \text{min.} & \boldsymbol{f}_{\boldsymbol{m}}^T \; E \; \boldsymbol{f}_m \\ \text{s.t.} & M_{11}\boldsymbol{v} + \boldsymbol{L}_r(\boldsymbol{q}, \dot{\boldsymbol{q}}) = W_g \boldsymbol{f}_m \\ & {\boldsymbol{f}_m}^{min} \leq \boldsymbol{f}_m \leq {\boldsymbol{f}_m}^{max} \end{array} \tag{13}$$

where E is a weighting matrix consisting of the physiological cross section areas of the muscles, and ${\boldsymbol{f}_m}^{min}$ and ${\boldsymbol{f}_m}^{max}$ are the lower and upper bounds on the muscle force magnitudes, respectively [30]. The cost function is the sum of squares of the muscle stresses [2].

2.4. Simulation of the framework

For a given desired (measured) rotational trajectory ($\boldsymbol{q}_{r_d}$), the developed framework allows forward-dynamics simulation of the GH joint model with 6 DOF (Fig. 3). The muscle force magnitudes ($\boldsymbol{f}_m$) are defined by the forward-dynamics framework such that the rotational generalized coordinates and velocities ($\boldsymbol{q}_r$ and $\dot{\boldsymbol{q}}_r$) of the GH joint follow their associated desired trajectories ($\boldsymbol{q}_{r_d}$ and $\dot{\boldsymbol{q}}_{r_d}$). The forward-dynamics framework consists of a feedforward and a feedback controller. The feedforward controller defines the gross control input based on (10), and the feedback controller has a fine action to compensate for

the tracking errors (12). The rotational motions of the joint together with the muscle forces that are applied to generate these rotational motions may lead to GH joint translations. The evolutions of these translations are captured through the 3 translational DOF ($\boldsymbol{q}_t$) of the GH joint model.

The deformable articular contact model defines the contact forces ($\boldsymbol{F}_c$). At each time step of the simulation, the contact force ($\boldsymbol{F}_c$) is defined as the resultant force of all the $\boldsymbol{f}_{c_i}$ forces. For the sake of computational efficiency of the simulation, a point search algorithm is developed using the techniques defining the intersection of two quadric surfaces [39]. Among all the $\boldsymbol{h}_i$ points constructing the humeral head surface, it provides at each time step a subset for which the penetration occurs. The contact model of (5) is smoothened using a continuous approximation of the heaviside function.

A smooth motion representing 150° abduction in the scapula plane is simulated. The motion is performed in 7.2 [s]. The Runge-Kutta-Fehlberg method [40], which combines a fourth and a fifth order Runge-Kutta scheme for error control is used to solve the equations of motion.

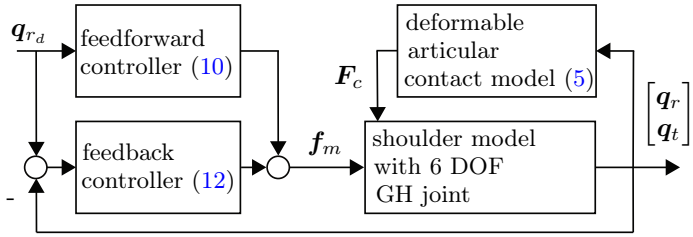

Figure 3: A block diagram representation of the developed framework. The contact force ($\boldsymbol{F}_c$) is defined by the deformable articular contact model (5). The muscle force magnitudes ($\boldsymbol{f}_m$) are defined by the feedforward (10) and the feedback (12) controller such that the 3 rotational DOF ($\boldsymbol{q}_r$) of the GH joint follow a given desired rotational trajectory ($\boldsymbol{q}_{r_d}$). The HHT is captured through the 3 translational DOF ($\boldsymbol{q}_t$).

The GH joint model with 6 DOF is evaluated for the simulated motion within the developed framework. The results are presented in terms of the HHT relative to the glenoid, the GH joint contact force, the contact area, the contact pressure on the glenoid cartilage, and the maximum normal strain of the glenoid cartilage. They are also compared with the associated results from the literature wherever it is possible. The evolution of the HHT is resolved along with the arm abduction in three directions of a frame attached to the glenoid fossa, including inferior-superior, posterior-anterior, and lateral-medial. The glenoid frame is constructed from the scapula frame (Fig. 2) by two transformations. First, the scapula frame is shifted by $(r_g - r_h)$ in the negative direction of z_s to the origin of the glenoid frame. It is then rotated along y_s and x_s to account for the glenoid fossa orientation according to [9]. A similar GH joint model but with 3 DOF (ideal ball-and socket) including the joint stability constraint is also simulated and its associated contact force is presented.

3. Results

The humeral head center translates relative to the glenoid frame from an inferior position superiorly until 90° abduction and then translates inferiorly (Fig. 4a). The range of inferior-superior HHT is around 2.5 [mm]. The humeral head center translates posteriorly from a central position and lies posteriorly throughout the simulated motion, whereas it translates anteriorly from 60° to 100° abduction (Fig. 4b). The range of posterior-anterior HHT is less than 0.5 [mm]. The humeral head center translates in the medial direction till 90° abduction and translates laterally afterward (Fig. 4c). The maximum HHT in the medial direction is less than 1.2 [mm].

The GH joint contact force increases to 660 [N] (87% of the bodyweight) at 90° abduction and decreases afterward (Fig. 5). The difference between the contact forces predicted by the 3 DOF and the 6 DOF GH joint model is less than 6%.

The contact area increases initially by the abduction and decreases afterward (Fig. 6). The distribution of the contact pressure applied on the glenoid cartilage varies by the arm abduction (Fig. 6). The maximum contact pressure increases from 0.50 [MPa] at 30° abduction by 130% at 90° abduction and decreases thereafter to almost its initial amount by the end of the motion. Positions on the glenoid fossa where the maximum contact pressure is applied (center of pressure) from 30° to 145° of the arm abduction lie in the superior-posterior quarter of the fossa.

The maximum normal strain of the glenoid cartilage increases from 0% at 0° abduction to almost 31% at 90° abduction that is around 1.1 [mm] of the thickness of the deformable layer covering the glenoid fossa (Fig. 7). It decreases afterward to almost 24% until the end of arm abduction.

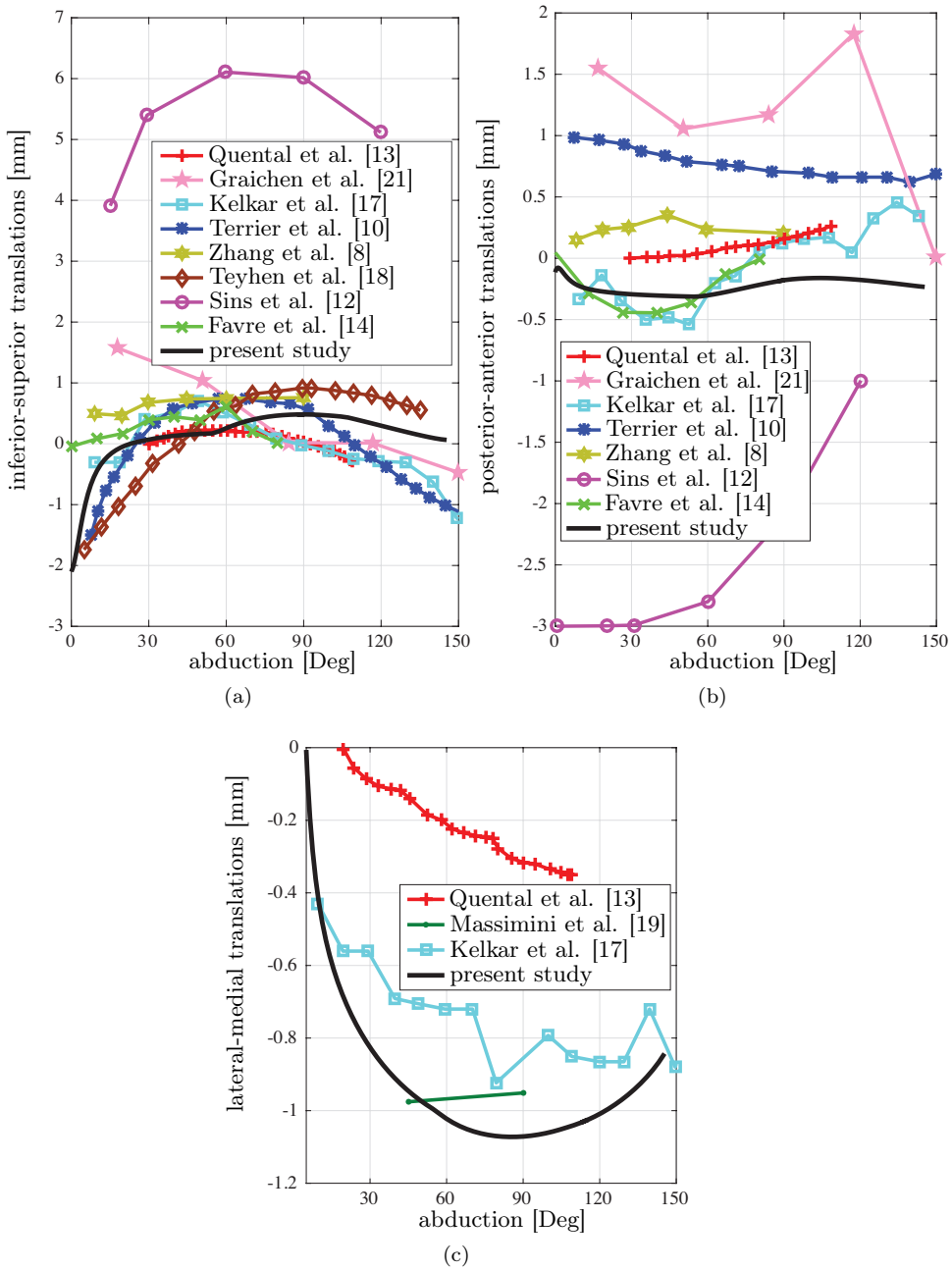

Figure 4: The HHT is resolved in three directions of the glenoid frame, namely inferior-superior (a), posterior-anterior (b), and lateral-medial (c). The associated results from the *in vitro* [17], *in vivo* [8, 18, 19, 21], and numerical [10, 12–14] studies are also shown.

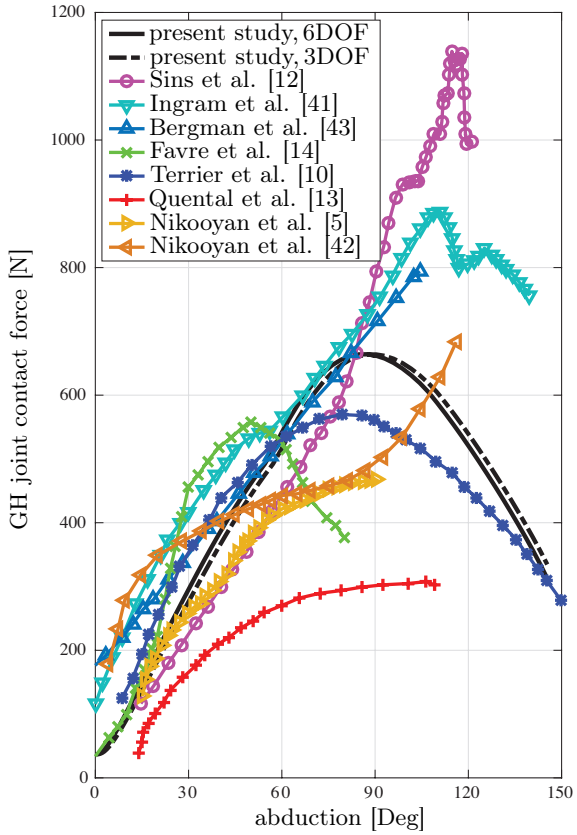

Figure 5: The GH joint contact force predicted by the present study and the associated results from numerical [5, 10, 12–14, 41, 42] and *in vivo* studies [43]. The results predicted by a similar GH joint model but with 3 DOF (ideal ball-and-socket) including the stability constraint is also shown.

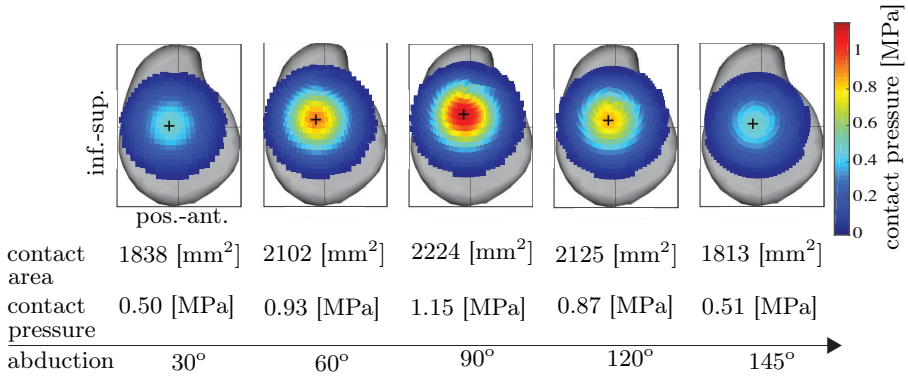

Figure 6: The distribution of the contact pressure applied on the glenoid cartilage and the contact area during the arm abduction. The results are shown for every 30° abduction. Positions on the glenoid fossa where the maximum contact pressure is applied (center of pressure) during the abduction are illustrated by black crosses.

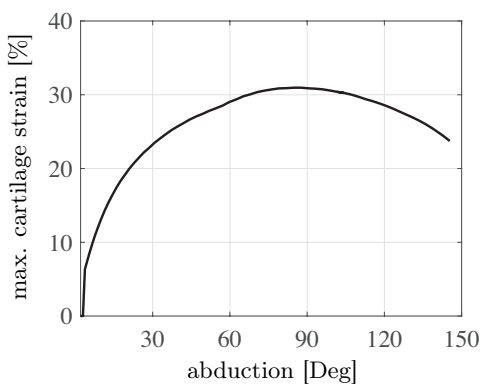

Figure 7: The maximum normal strain of the glenoid cartilage varies with the arm abduction.

4. Discussion

The aim of this study was to develop a simulation framework that allowed forward-dynamics simulation of a shoulder model consisting of a GH joint with 6 DOF associated to rotations and translations of the humerus in the glenoid fossa. The model thus provided the HHT during controlled elevation of the arm. We showed that a forward-dynamics framework addressing HHT required extra information about the glenohumeral contact. To that end, a deformable articular contact was included, providing a mapping from the generalized coordinates and velocities to the contact forces. The simulation framework was tested and verified during a movement of abduction in the scapula plane. We specifically analyzed the HHT, the GH joint contact force, the contact area, the

contact pressure, and the cartilage strain. These results were indirectly validated through comparison with *in vivo*, *in vitro*, and other numerical studies.

The initial inferior position of the humeral head center can be explained by the fact that the passive structures (ligaments, capsule, and labrum) surrounding the GH joint are lax when the joint is in its neutral configuration. Then until 30° abduction, the humeral head center experienced a superior translations that placed it in a rather central position. This was due to an upward pull by the muscles that has been already reported in [44, 45]. The upward pull was compensated by the contact force, producing a cartilage deformation (about 22% strain). After this first phase, the humeral head center remained in the superior-posterior quarter of the glenoid fossa.

A large variability of HHT was reported in the literature. Therefore, a rigorous validation of the HHT estimated by our framework was not possible. However, the trend of predicted inferior-superior HHT was consistent with the most commonly reported pattern ([10, 12, 13, 17, 18]). The range of translation also corresponded well with the literature ([18], [8], and [17]).

The difference in curvature radii of joint articulating surfaces often defines the joint congruence. An incongruence of 2 [mm] was assumed in this study for the GH joint based on observations of clinical studies, e.g. [17, 29]. However, some authors claimed the GH joint to be perfectly congruent (same radii) [46]. We found a correlation between the incongruence of the GH joint and the inferior-superior translations. That is, a larger difference in the radii of the humeral head and the glenoid fossa results in larger predicted translations in the inferior-superior direction. For the case of congruent joint, the translations were still witnessed but with much smaller amplitudes in the inferior-superior direction. Furthermore, we found that neither posterior-anterior translations nor lateral-medial translations were correlated with the GH joint incongruence. These findings are consistent with clinical and numerical observations reported in the literature, e.g. [17, 47, 48].

The predicted GH joint contact force was consistent with *in vivo* measurements of instrumented prostheses [43] and the other numerical predictions [5, 10, 12, 41, 42], at least up to 90° abduction. There was less than 8% difference between our estimation of the contact force at 90° abduction and measurements of instrumented prostheses. However, it should be mentioned that there are yet a number of limitations concerning applications of instrumented prostheses to validate estimated joint contact forces. Particularly, the post-surgery patients who participated in the *in vivo* study of [43] had compromised arm range of motions (ROM). Their musculotendinous were also damaged or disrupted possibly due to the associated surgeries. Furthermore, they might have had pathological neuromuscular motor control stemming from pain or compromised ROM. Therefore, their muscular functions, joint kinematics, and joint mechanics (contact forces) differed from those of healthy subjects.

After 90° abduction, there is no clear consensus between the contact forces estimated by the different studies mentioned above. Inter-individual morphological differences and models shortcoming in replicating specific motor control of subjects seem to be potential sources of this inconsistency. Subject-specific

modeling together with inclusion of measured EMG signals provided noticeable improvements [42, 49]. Nevertheless, we indeed observed that contact pressure decreased after 90° abduction. Therefore, the contact force can be expected to exhibit the same descending behavior after 90° abduction.

The simulation of the 3 DOF GH joint model including the stability constraint and the 6 DOF GH joint model showed that the difference in the estimated maximum contact forces was indeed negligible during the slow abduction. This fully supports the well accepted ideal ball-and-socket approximation of the GH joint with the stability constraint for applications requiring force estimations. However, as a recommendation for future works, it would be interesting to quantify this difference for simulation of activities of daily living (ADL). The muscle force prediction of the 3 DOF model including the stability constraint was already validated against EMG measurements in our previous work [50].

A discrepancy exists between the predicted contact area and *in vitro* measurements ([51, 52]). For instance, the predicted contact area was on average almost 2.8 and 4 times larger than the experimental measurements reported in [51] and [52], respectively. However, given the practical differences in the definition of contact between our approach and the *in vitro* studies, the observed discrepancy was expected. In our model, any infinitesimal surface on the humeral head with an infinitesimal penetration in the glenoid fossa was considered to be in contact. On the other hand, in the *in vitro* studies the definition of contact is subject to measurement precision. In a real joint, we can reasonably assume a full contact between the two deformable cartilage layers.

The predicted contact pressure was consistent with the literature, e.g. [14, 52]. For example, the maximum contact pressure predicted by our framework and the *in vitro* study in [52] at 60° was 0.93 [MPa] and 0.91 [MPa], respectively. The predicted center of pressure in the superior-posterior quarter of the glenoid fossa was also consistent with the literature [12, 14, 18].

The application of forward-dynamics simulation together with the deformable articular contact model allowed us to solve the differential equations of motion of the GH joint with 6 DOF. Therefore, the dynamic effects of motion were naturally included in the translations predicted by our framework. Indeed, the first and second derivatives of the translational degrees of freedom were neglected in the previous studies (e.g. [9, 12, 14]) in order to transform the differential equations of motion to a set of algebraic equations.

The indeterminacy associated with the unknown contact force was resolved by incorporating a function mapping that defined the unknown contact force in terms of the joint kinematics. The function mapping was defined using a viscoelastic contact model. However, the necessity of incorporating a function mapping to resolve the indeterminacy should be distinguished from the methodology used to find this function mapping. In other words, a function mapping that defines the unknown contact force in terms of the joint kinematics is necessary to resolve the indeterminacy. However, there are several methodologies to define such a function mapping. For instance, given the viscoelastic characteristic of the *in vivo* GH joint, we used a viscoelastic contact model to define the associated function mapping. Whereas, one can consider an elastic contact

model or a friction model to find an associated function mapping.

The developed framework included a multibody musculoskeletal model together with a representation of the cartilage contact mechanics. It therefore provided an integrated solution to study the relationship between joint kinematics, muscle forces, and cartilage stress. The common approach in the literature consists of two steps. First, a musculoskeletal model is used to define the rotational joint kinematics as well as the muscle forces. Then, a finite element analysis is performed to define the translational joint kinematics and the cartilage stress based on the results provided from the first step.

One of the limitations of the present study was linked to the fact that we focussed on the GH joint itself without considering the effect of the adjacent bones. Future development should therefore incorporate a large-scale model of the shoulder into the framework. The second limitation referred to the spherical approximation of the humeral head. However, it is straightforward to integrate more realistic anatomical geometries in the developed framework. The third limitation was associated with neglecting the GH joint passive structures (ligaments, capsule, and labrum) in the evaluated shoulder model. However, given that they are lax except for the extreme positions of the joint [45], their contribution for the simulated motion was expected to be negligible. Furthermore, to simulate motions involving the joint extreme positions, inclusion of these passive structures in the framework is necessary. To this end, a model of the passive structures defining their associated force as a function of joint kinematics (e.g. see [53]), could be integrated in the framework in our future developments. Another limitation was related to the fact that the articular contact was approximated as a rigid-to-deformable contact (rigid humeral head in contact with the deformable glenoid fossa). It simplified the formulation of the contact problem provided that the deformation of one contacting component was only involved. However, this deviated from the more complex deformable-to-deformable contact of the *in vivo* GH joint.

In conclusion, we developed a framework based on a joint application of a forward-dynamics simulation and a deformable articular contact to simulate a human shoulder model including a 6 DOF GH joint model. It not only provided estimations of muscle and joint reaction forces (similar to 3 DOF GH joint models) but also allowed estimations of HHT, contact areas, and contact pressure. The latter is required to broaden our understanding of the GH joint stability and more crucially to design shoulder prostheses. This novel framework had three main advantages. First, given that the dynamic equations of motion were solved forward in time, the dynamic effects of motion were naturally considered despite the previous numerical [9, 11, 12, 14, 15] and *in vivo* [8, 19, 21] studies. Second, a nonlinear viscoelastic approximation was used for the articular contact. Third, it provided an integrated solution for the study of the GH joint function that dealt simultaneously with the joint kinematics and mechanics. The results were in a good agreement with the ones from the literature. In a next step, the proposed framework could be populated with subject-specific morphological data to account for effects of inter-individual anatomical variabilities on GH joint functions during ADL. The proposed methodology could also

be translated for clinical applications related to the treatment of osteoarthritis by TSA. Furthermore, outcomes of the proposed simulation framework could be applied for biomechanical analysis and design of available and forthcoming shoulder prostheses.

Acknowledgment

This project was supported by the Swiss National Science Foundation [K-32K1-122512].

References

[1] J. A. Prinold, M. Masjedi, G. R. Johnson, A. M. Bull, Musculoskeletal shoulder models: a technical review and proposals for research foci, Proceedings of the Institution of Mechanical Engineers, Part H: Journal of Engineering in Medicine (2013) 0954411913492303.

[2] B. A. Garner, M. G. Pandy, Musculoskeletal model of the upper limb based on the visible human male dataset, Computer methods in biomechanics and biomedical engineering 4 (2) (2001) 93–126.

[3] D. Ingram, C. Engelhardt, A. Farron, A. Terrier, P. Müllhaupt, Modelling of the human shoulder as a parallel mechanism without constraints, Mechanism and Machine Theory 100 (2016) 120–137.

[4] I. W. Charlton, G. Johnson, A model for the prediction of the forces at the glenohumeral joint, Proceedings of the Institution of Mechanical Engineers, Part H: Journal of Engineering in Medicine 220 (8) (2006) 801–812.

[5] A. A. Nikooyan, H. Veeger, E. Chadwick, M. Praagman, F. C. van der Helm, Development of a comprehensive musculoskeletal model of the shoulder and elbow, Medical & biological engineering & computing 49 (12) (2011) 1425–1435.

[6] M. Damsgaard, J. Rasmussen, S. T. Christensen, E. Surma, M. De Zee, Analysis of musculoskeletal systems in the anybody modeling system, Simulation Modelling Practice and Theory 14 (8) (2006) 1100–1111.

[7] K. R. Holzbaur, W. M. Murray, S. L. Delp, A model of the upper extremity for simulating musculoskeletal surgery and analyzing neuromuscular control, Annals of biomedical engineering 33 (6) (2005) 829–840.

[8] C. Zhang, W. Skalli, P.-Y. Lagacé, F. Billuart, X. Ohl, T. Cresson, N. J. Bureau, D. M. Rouleau, A. Roy, P. Tétreault, et al., Investigation of 3d glenohumeral displacements from 3d reconstruction using biplane x-ray images: Accuracy and reproducibility of the technique and preliminary analysis in rotator cuff tear patients, Journal of Electromyography and Kinesiology.

[9] A. Terrier, A. Vogel, M. Capezzali, A. Farron, An algorithm to allow humerus translation in the indeterminate problem of shoulder abduction, Medical engineering & physics 30 (6) (2008) 710–716.

[10] A. Terrier, X. Larrea, V. M. Camine, D. Pioletti, A. Farron, Importance of the subscapularis muscle after total shoulder arthroplasty, Clinical Biomechanics 28 (2) (2013) 146–150.

[11] A. R. Hopkins, U. N. Hansen, A. A. Amis, M. Taylor, N. Gronau, C. Anglin, Finite element modelling of glenohumeral kinematics following total shoulder arthroplasty, Journal of biomechanics 39 (13) (2006) 2476–2483.

[12] L. Sins, P. Tétreault, N. Hagemeister, N. Nuño, Adaptation of the anybody™ musculoskeletal shoulder model to the nonconforming total shoulder arthroplasty context, Journal of biomechanical engineering 137 (10) (2015) 101006.

[13] C. Quental, J. Folgado, J. Ambrósio, J. Monteiro, A new shoulder model with a biologically inspired glenohumeral joint, Medical Engineering & Physics 38 (9) (2016) 969–977.

[14] P. Favre, M. Senteler, J. Hipp, S. Scherrer, C. Gerber, J. G. Snedeker, An integrated model of active glenohumeral stability, Journal of biomechanics 45 (13) (2012) 2248–2255.

[15] P. Büchler, N. Ramaniraka, L. Rakotomanana, J. Iannotti, A. Farron, A finite element model of the shoulder: application to the comparison of normal and osteoarthritic joints, Clinical Biomechanics 17 (9) (2002) 630–639.

[16] N. Wuelker, H. Schmotzer, K. Thren, M. Korell, Translation of the glenohumeral joint with simulated active elevation., Clinical orthopaedics and related research 309 (1994) 193–200.

[17] R. Kelkar, V. M. Wang, E. L. Flatow, P. M. Newton, G. A. Ateshian, L. U. Bigliani, R. J. Pawluk, V. C. Mow, Glenohumeral mechanics: a study of articular geometry, contact, and kinematics, Journal of Shoulder and Elbow Surgery 10 (1) (2001) 73–84.

[18] D. S. Teyhen, T. R. Christ, E. R. Ballas, C. W. Hoppes, J. D. Walters, D. S. Christie, G. Dreitzler, E. J. Kane, Digital fluoroscopic video assessment of glenohumeral migration: Static vs. dynamic conditions, Journal of biomechanics 43 (7) (2010) 1380–1385.

[19] D. F. Massimini, P. J. Boyer, R. Papannagari, T. J. Gill, J. P. Warner, G. Li, In-vivo glenohumeral translation and ligament elongation during abduction and abduction with internal and external rotation, Journal of orthopaedic surgery and research 7 (1) (2012) 1.

[20] W. Sahara, K. Sugamoto, M. Murai, H. Tanaka, H. Yoshikawa, The three-dimensional motions of glenohumeral joint under semi-loaded condition during arm abduction using vertically open mri, Clinical Biomechanics 22 (3) (2007) 304–312.

[21] H. Graichen, T. Stammberger, H. Bonel, K.-H. Englmeier, M. Reiser, F. Eckstein, Glenohumeral translation during active and passive elevation of the shoulder—a 3d open-mri study, Journal of biomechanics 33 (5) (2000) 609–613.

[22] N. Nishinaka, H. Tsutsui, K. Mihara, K. Suzuki, D. Makiuchi, Y. Kon, T. W. Wright, M. W. Moser, K. Gamada, H. Sugimoto, et al., Determination of in vivo glenohumeral translation using fluoroscopy and shape-matching techniques, Journal of Shoulder and Elbow Surgery 17 (2) (2008) 319–322.

[23] M. J. Bey, S. K. Kline, R. Zauel, T. R. Lock, P. A. Kolowich, Measuring dynamic in-vivo glenohumeral joint kinematics: technique and preliminary results, Journal of biomechanics 41 (3) (2008) 711–714.

[24] M. S. Andersen, M. Damsgaard, J. Rasmussen, Force-dependent kinematics: a new analysis method for non-conforming joints, in: 13th Biennial International Symposium on Computer Simulation in Biomechanics, 2011.

[25] C. Quental, J. Folgado, J. Ambrósio, J. Monteiro, A multibody biomechanical model of the upper limb including the shoulder girdle, Multibody System Dynamics 28 (1-2) (2012) 83–108.

[26] D. P. Pioletti, L. Rakotomanana, J.-F. Benvenuti, P.-F. Leyvraz, Viscoelastic constitutive law in large deformations: application to human knee ligaments and tendons, Journal of biomechanics 31 (8) (1998) 753–757.

[27] A. Terrier, A. Reist, A. Vogel, A. Farron, Effect of supraspinatus deficiency on humerus translation and glenohumeral contact force during abduction, Clinical Biomechanics 22 (6) (2007) 645–651.

[28] A. Terrier, F. Merlini, D. P. Pioletti, A. Farron, Total shoulder arthroplasty: downward inclination of the glenoid component to balance supraspinatus deficiency, Journal of shoulder and elbow surgery 18 (3) (2009) 360–365.

[29] L. J. Soslowsky, E. L. Flatow, L. U. Bigliani, V. C. Mow, Articular geometry of the glenohumeral joint., Clinical orthopaedics and related research 285 (1992) 181–190.

[30] A. Terrier, M. Aeberhard, Y. Michellod, P. Mullhaupt, D. Gillet, A. Farron, D. P. Pioletti, A musculoskeletal shoulder model based on pseudo-inverse and null-space optimization, Medical engineering & physics 32 (9) (2010) 1050–1056.

[31] H. Baruh, Analytical dynamics, WCB/McGraw-Hill Boston, 1999.

[32] D. T. Greenwood, Advanced dynamics, Cambridge University Press, 2006.

[33] T. M. Guess, H. Liu, S. Bhashyam, G. Thiagarajan, A multibody knee model with discrete cartilage prediction of tibio-femoral contact mechanics, Computer methods in biomechanics and biomedical engineering 16 (3) (2013) 256–270.

[34] L. Blankevoort, J. Kuiper, R. Huiskes, H. Grootenboer, Articular contact in a three-dimensional model of the knee, Journal of biomechanics 24 (11) (1991) 1019–1031.

[35] J. E. Novotny, B. D. Beynnon, C. E. Nichols, Modeling the stability of the human glenohumeral joint during external rotation, Journal of Biomechanics 33 (3) (2000) 345–354.

[36] E. Sarshari, A. Farron, A. Terrier, D. Pioletti, P. Müllhaupt, A framework for forward-dynamics simulation of the human shoulder, in: 11th Conference of the International Shoulder Group, ISG 2016, no. EPFL-CONF-218098, 2016.

[37] M. W. Spong, Modeling and control of elastic joint robots, Journal of dynamic systems, measurement, and control 109 (4) (1987) 310–318.

[38] J.-J. E. Slotine, W. Li, et al., Applied nonlinear control, Vol. 199, prentice-Hall Englewood Cliffs, NJ, 1991.

[39] I. Wilf, Y. Manor, Quadric-surface intersection curves: shape and structure, Computer-Aided Design 25 (10) (1993) 633–643.

[40] J. R. Dormand, Numerical methods for differential equations: a computational approach, Vol. 3, CRC Press, 1996.

[41] D. Ingram, C. Engelhardt, A. Farron, A. Terrier, P. Müllhaupt, Improving anterior deltoid activity in a musculoskeletal shoulder model–an analysis of the torque-feasible space at the sternoclavicular joint, Computer methods in biomechanics and biomedical engineering 19 (4) (2016) 450–463.

[42] A. Nikooyan, H. Veeger, P. Westerhoff, B. Bolsterlee, F. Graichen, G. Bergmann, F. Van der Helm, An emg-driven musculoskeletal model of the shoulder, Human movement science 31 (2) (2012) 429–447.

[43] G. Bergmann, F. Graichen, A. Bender, M. Kääb, A. Rohlmann, P. Westerhoff, In vivo glenohumeral contact forces—measurements in the first patient 7 months postoperatively, Journal of biomechanics 40 (10) (2007) 2139–2149.

[44] E. Sarshari, D. Ingram, C. A. Engelhardt, A. Farron, D. Pioletti, A. Terrier, P. Müllhaupt, Active stability of glenohumeral joint diminishes during the end-range motions, in: ESB15-0089, no. EPFL-CONF-205110, 2015.

[45] T. Yanagawa, C. J. Goodwin, K. B. Shelburne, J. E. Giphart, M. R. Torry, M. G. Pandy, Contributions of the individual muscles of the shoulder to glenohumeral joint stability during abduction, Journal of biomechanical engineering 130 (2) (2008) 021024.

[46] F. C. Van der Helm, H. Veeger, G. Pronk, L. Van der Woude, R. Rozendal, Geometry parameters for musculoskeletal modelling of the shoulder system, Journal of biomechanics 25 (2) (1992) 129–144.

[47] R. Oosterom, J. Herder, F. van der Helm, W. Święszkowski, H. Bersee, Translational stiffness of the replaced shoulder joint, Journal of biomechanics 36 (12) (2003) 1897–1907.

[48] C. Anglin, U. P. Wyss, D. R. Pichora, Shoulder prosthesis subluxation: theory and experiment, Journal of Shoulder and Elbow Surgery 9 (2) (2000) 104–114.

[49] W. Wu, P. V. Lee, A. L. Bryant, M. Galea, D. C. Ackland, Subject-specific musculoskeletal modeling in the evaluation of shoulder muscle and joint function, Journal of Biomechanics 49 (15) (2016) 3626–3634.

[50] C. Engelhardt, A. Farron, F. Becce, N. Place, D. P. Pioletti, A. Terrier, Effects of glenoid inclination and acromion index on humeral head translation and glenoid articular cartilage strain, Journal of Shoulder and Elbow Surgery.

[51] L. Soslowsky, E. Flatow, L. Bigliani, R. Pawluk, G. Ateshian, V. Mow, Quantitation of in situ contact areas at the glenohumeral joint: a biomechanical study, Journal of Orthopaedic Research 10 (4) (1992) 524–534.

[52] G. Hammond, J. E. Tibone, M. H. McGarry, B.-J. Jun, T. Q. Lee, Biomechanical comparison of anatomic humeral head resurfacing and hemiarthroplasty in functional glenohumeral positions, The Journal of Bone & Joint Surgery 94 (1) (2012) 68–76.

[53] R. Debski, E. Wong, S. L. Woo, F. Fu, J. Warner, An analytical approach to determine the in situ forces in the glenohumeral ligaments, Journal of biomechanical engineering 121 (3) (1999) 311–315.